VALIDATION OF CFD MODELS FOR MONO- AND POLYDISPERSE AIR-WATER TWO-PHASE FLOWS IN PIPES

Th. Frank[1], P.J. Zwart[2],

E. Krepper[3], H.-M. Prasser[3], D. Lucas[3]

[1]ANSYS Germany GmbH, Staudenfeldweg 12, D-83624 Otterfing, Germany
Phone: +49 (8024) 9054 76, Fax: +49 (8024) 9054 33
Thomas.Frank@ansys.com
[2]ANSYS Canada Ltd., 554 Parkside Drive, Waterloo, Ontario N2L 5Z4, Canada
[3]FZ Rossendorf – Institute of Safety Research, P.Box 510119, D-01314 Dresden, Germany

Abstract

Many flow regimes in Nuclear Reactor Safety (NRS) Research are characterized by multiphase flows, where one of the phases is continuous and the other phase consists of gas or vapor of the liquid phase. The validation of the CFD multiphase flow models against detailed experimental data for simplified flow configurations is a basic requirement for the accurate prediction of more complex flows, like e.g. multiphase flow in fuel rod assemblies with spacer grids under the conditions from ONB to DNB including bulk and wall boiling in a pressurized polydisperse liquid-vapor flow. This paper is therefore aimed on validation of the underlying multiphase flow modeling concepts for gas-liquid monodisperse and polydisperse bubbly flows. CFD predictions using ANSYS CFX and taking into account interphase momentum transfer (drag and non-drag forces) as well as bubble break-up and coalescence are compared to experiments of MT-Loop and TOPFLOW test facilities (FZ Rossendorf, Germany). Best Practice Guidelines [8] have been applied in order to allow for a systematic error quantification and thoroughly assessment of model formulations.

[1] Corresponding author

Introduction

Many flow regimes in Nuclear Reactor Safety (NRS) Research are characterized by multiphase flows, where one of the phases is continuous and the other phase consists of gas or vapor of the liquid phase. The validation of the CFD multiphase flow models against detailed experimental data for simplified flow configurations is a basic requirement for the accurate prediction of more complex flows. Investigations of gas-liquid two-phase flows presented in this paper therefore start from a simple vertical pipe flow in the regime of monodisperse bubbly flow (MT-Loop 074 test case). More complexity is added to the model validation step-by-step, introducing the inhomogeneous MUSIG model for the treatment of bubbly and slug flows with broader size distribution of the gaseous phase geometrical scales and bubble break-up and coalescence. Further investigations had been carried out on gas-liquid two-phase flows with transient changes in the flow regime, superficial velocities and gas void fractions as well as on complex 3-dimensional gas-liquid flows around obstacles for turbulence model validation purposes. Due to constraints on the size of this paper, these investigations are not included here. The future aim of the multiphase flow model development in ANSYS CFX is a further enhancement towards fully compressible vapor-liquid two-phase flows with mass, momentum and heat transfer under high temperature and pressure in order to be able to predict more complex flows with high relevance to nuclear reactor safety research, like e.g. multiphase flow in large break LOCA or multiphase flow in fuel rod assemblies with spacer grids under the conditions from ONB[2] to DNB[3] including bulk boiling, wall boiling and conjugate heat transfer to walls in a pressurized polydisperse liquid-vapor flow.

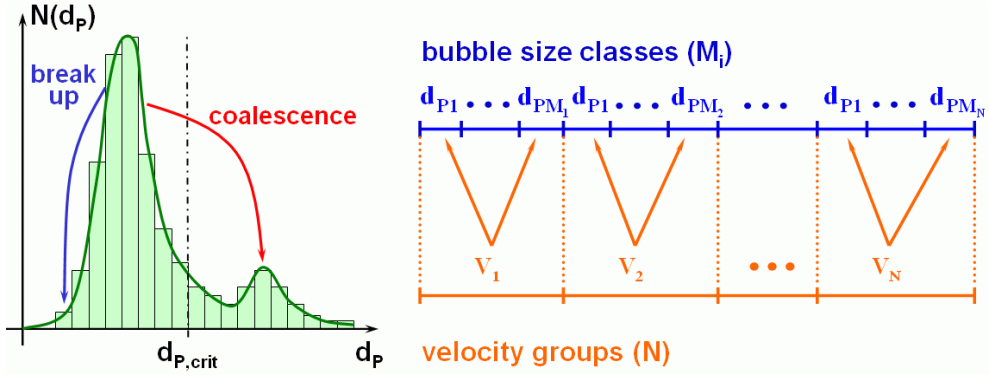

Fig. 1: Velocity group and bubble size class subdivision of the bubble size spectrum in the inhomogeneous MUSIG model for polydisperse bubbly flow.

The Multi-Fluid Model for Disperse Gas-Liquid Flows

Velocity Groups and Bubble Size Classes

Monodisperse bubbly flow can be characterized by a single geometrical scale of the disperse gaseous phase – the bubble diameter. Subsequently a two-phase flow model can be formulated describing the liquid and gaseous phase velocity fields and gas void fraction distribution. For a

[2] ONB – Onset of Nucleate Boiling
[3] DNB – Departure of Nucleate Boiling

polydisperse bubbly or slug flow with more then a single geometrical scale of the gaseous phase it has been shown by Tomiyama [13], that the lift force acting on bubbles is changing its direction in dependence on bubble size leading to a radial demixing of differently sized bubbles in vertical pipes. This radial demixing of small and large bubbles with respect to the critical bubble diameter in Tomiyama's lift force coefficient correlation can only be captured by a multiphase flow model, if differently sized bubbles are allowed to move with different velocity fields.

Therefore in the proposed inhomogeneous Multiple Size Group (MUSIG) model the gaseous disperse phase is divided into a number N so-called velocity groups (or phases), where each of the velocity groups is characterized by its own velocity field. The subdivision should be based on the physics of bubble motion for bubbles of different size, e.g. different behavior of differently sized bubbles with respect to lift force or turbulent dispersion. Therefore it can be suggested, that in most cases 3 or 4 velocity groups should be sufficient in order to capture the main phenomena in bubbly or slug flows.

Further the overall bubble size distribution is represented by dividing the bubble diameter range within each of the velocity groups in a number M_i bubble size classes (Fig. 1). The lower and upper boundaries of bubble diameter intervals for the bubble size classes can be controlled by either an equal bubble diameter distribution, an equal bubble mass distribution or can be based on user definition of the bubble diameter ranges for each distinct bubble diameter class. For simplicity it is further assumed, that the number of bubble diameter classes within each of the velocity groups is equal, i.e. $M=M_1= M_2= \ldots= M_N$, also this is not a limitation of the model.

Model Formulation

The simulation of the gas-liquid monodispersed or polydispersed bubbly flows is based on the CFX-10 multi-fluid Euler-Euler approach [2]. The Eulerian modeling framework is based on ensemble-averaged mass and momentum transport equations for all phases/velocity groups. Regarding the liquid phase as continuum ($\alpha=1$) and the gaseous phase velocity groups (bubbles) as disperse phase ($\alpha=2,\ldots,N+1$) these equations read:

$$\frac{\partial}{\partial t}\left(r_\alpha \rho_\alpha\right)+\nabla.\left(r_\alpha \rho_\alpha \vec{U}_\alpha\right)=S_\alpha \tag{1}$$

$$\frac{\partial}{\partial t}\left(r_\alpha \rho_\alpha \vec{U}_\alpha\right)+\nabla.\left(r_\alpha \rho_\alpha \vec{U}_\alpha \otimes \vec{U}_\alpha\right)= \nabla.\left(r_\alpha \mu_\alpha (\nabla \vec{U}_\alpha + (\nabla \vec{U}_\alpha)^T)\right) - r_\alpha \nabla p + r_\alpha \rho_\alpha \vec{g} + \vec{M}_\alpha + \vec{S}_{M\alpha} \tag{2}$$

$$\vec{M}_\alpha = \vec{F}_D + \vec{F}_L + \vec{F}_{WL} + \vec{F}_{TD} \tag{3}$$

where r_α, ρ_α, μ_α are the void fraction, density and viscosity of the phase α and $\vec{M}_\alpha$ represents the sum of interfacial forces like the drag force $\vec{F}_D$, lift force $\vec{F}_L$, wall lubrication force $\vec{F}_{WL}$ and turbulent dispersion force $\vec{F}_{TD}$. The source terms S_α and $\vec{S}_{M\alpha}$ represent the transfer of gaseous phase mass and momentum between different velocity groups due to bubble break-up and coalescence processes leading to bubbles of certain size belonging to a different velocity group. Consequently these terms are zero for the liquid phase transport equations. Equations for a monodisperse bubbly flow appear to be a special case of eq.s (1)-(3) for N=1 and $S_\alpha= \vec{S}_{M\alpha}=0$. Turbulence of the liquid phase has been modeled using Menter's k-ω based Shear Stress Transport (SST) model [2]. The turbulence of the disperse bubbly phase was modeled

using a zero equation turbulence model and bubble induced turbulence has been taken into account according to Sato's model [2].

The interfacial drag and non drag force terms M_β can be written as:

$$\vec{F}_D = \frac{3}{4} C_D \frac{r_\beta \rho_\alpha}{d_\beta} \left| \vec{U}_\alpha - \vec{U}_\beta \right| (\vec{U}_\alpha - \vec{U}_\beta) \tag{4}$$

$$\vec{F}_L = C_L r_\beta \rho_\alpha (\vec{U}_\alpha - \vec{U}_\beta) \times \nabla \times \vec{U}_\alpha \tag{5}$$

$$\vec{F}_{WL} = -C_{WL} r_\beta \rho_\alpha \left| \vec{U}_{rel} - (\vec{U}_{rel} \cdot \vec{n}_W) \vec{n}_W \right|^2 \vec{n}_W \tag{6}$$

RPI turbulent dispersion force model:

$$\vec{F}_{TD} = -C_{TD} \rho_L k_L \nabla r_G \tag{7}$$

Favre-averaged-drag (FAD) turbulent dispersion force model:

$$\vec{F}_{TD} = D_{\alpha\beta} A_{\alpha\beta} \frac{\nu_{t\alpha}}{\sigma_{r\alpha}} \left(\frac{\nabla r_\alpha}{r_\alpha} - \frac{\nabla r_\beta}{r_\beta} \right) \tag{8}$$

Here α denotes the liquid phase and β the properties of the corresponding gaseous phase velocity group. These interfacial momentum transfer terms need further closure relations for the various force coefficients C_D, C_L, C_{WL}, C_{TD} and model parameters like $\sigma_{r\alpha}$. In the present study the Grace [2] and Tomiyama drag coefficient [14], Tomiyama lift force coefficient [13] and the so-called Favre-averaged-drag (FAD) turbulent dispersion model [4] were used. The Tomiyama drag force coefficient correlation considers bubble drag in the distorted bubble regime similar to the Grace drag model built into ANSYS CFX, but additionally contains a parameter considering the contamination of the air-water system. This contamination parameter has been set to A=24 and the high gas void fraction correction exponent was set to n=4 as recommended by the author of the Tomiyama drag correlation [14]. The lift force coefficient $C_L = C_L(\mathrm{Eo}_d)$ has been determined in accordance with the correlation for deformable bubbles number published by Tomiyama [13] as a function of the bubble Eötvös number:

$$C_L = \begin{cases} \min\left[0.288 \tanh(0.121 \mathrm{Re}_P), f(Eo_d)\right], & Eo_d < 4 \\ f(Eo_d), & 4 \le Eo_d \le 10 \\ -0.27, & Eo_d > 10 \end{cases} \tag{9}$$

with:

$$f(Eo_d) = 0.00105 Eo_d^3 - 0.0159 Eo_d^2 - 0.0204 Eo_d + 0.474 \tag{10}$$

where Eo_d is the Eötvös number based on the long axis d_H of a deformable bubble, i.e.:

$$Eo_d = \frac{g(\rho_L - \rho_G) d_H^2}{\sigma} \quad , \quad d_H = d_P (1 + 0.163 Eo)^{1/3} \quad , \quad Eo = \frac{g(\rho_L - \rho_G) d_P^2}{\sigma} \tag{11}$$

The given correlation of eq. (9) takes into account bubble deformation and asymmetric wake effects on bubble lift and leads to a sign change of the lift force for bubbles with a diameter of $d_P > 5.5mm$ for air bubbles in water under normal conditions. The critical bubble diameter, where the sign change of the lift force occurs, strongly depends on the bubble surface tension and shifts towards smaller bubble diameters of about $d_P \sim 3.5mm$ for e.g. a vapor-water system under higher pressure of about 65bar and at saturation temperature. The bubble size dependent bubble lift force leads further to the fact, that in a polydisperse bubbly flow bubbles of different diameter tend to separate. This bubble separation effects cannot be described in the framework of

a two-phase flow model with a single gaseous phase velocity field. The later described inhomogeneous MUSIG model has been developed in order to take into account such bubble separation effects induced by the bubble lift force in dependence on the bubble size distribution.

For the wall lubrication force model the formulations of Antal [1]:

$$C_{WL} = \max\left\{0, \frac{C_{W1}}{d_P} + \frac{C_{W2}}{y_W}\right\} \tag{12}$$

with y_W being the wall distance and recommended values of C_{W1}=-0.01 and C_{W2}=0.05 as well as the formulation of Tomiyama [13]:

$$C_{WL} = C_{W3}\frac{d_P}{2}\left(\frac{1}{y_W^2} - \frac{1}{(D-y_W)^2}\right) \tag{13}$$

with D being the pipe diameter and:

$$C_{W3} = \begin{cases} e^{-0.933Eo+0.179} & 1 \le Eo \le 5 \\ 0.00599Eo - 0.0187 & 5 < Eo \le 33 \\ 0.179 & 33 < Eo \end{cases} \tag{14}$$

have been used. From validation simulations it could be shown, that both formulations of Antal and Tomiyama have disadvantages. While the Antal formulation is geometry independent, it can be shown from numerical simulations that the formulation fails under certain flow conditions because the wall lubrication force predicted by eq. (6) and (12) is too small in order to balance strong lift forces arising from eq. (5). The Tomiyama formulation for the wall lubrication force from eq. (6), (13) and (14) leads to improved prediction of gaseous phase volume fraction profiles for a wider range of flow conditions. But the formulation is limited to pipe flow investigations since it contains the pipe diameter as a geometry length scale. In order to derive a geometry independent formulation for the wall lubrication force while preserving the general behavior of Tomiyama's formulation, the author [5] supposes a generalized formulation for the wall lubrication force as follows:

$$C_{WL} = C_{W3}(Eo)\cdot\max\left\{0, \frac{1}{C_{WD}}\cdot\frac{1-\frac{y_W}{C_{WC}d_P}}{y_W\cdot\left(\frac{y_W}{C_{WC}d_P}\right)^{p-1}}\right\} \tag{15}$$

with the cut-off coefficient C_{WC}, the damping coefficient C_{WD} and a variable potential law for $F_{WL} \sim 1/y_W^{p-1}$. The Eötvos number dependent coefficient $C_{W3}(Eo)$ is determined from eq. (14)preserving the dependency on bubble surface tension. From numerical simulations it was found, that a good agreement with experimental data can be obtained for C_{WC}=10.0, C_{WD}=6.8 and p=1.7. Thereby the introduction of an additional geometrical length scale can be avoided, which can be hardly correctly defined in arbitrary geometries.

The given non-drag forces were implemented in ANSYS CFX. Other drag and non-drag force models can be implemented as well using user defined CFX command language (CCL) expressions or FORTRAN routines for the prediction of the various force coefficients.

Bubble Break-up and Coalescence

In the inhomogeneous MUSIG model the polydispersed gaseous phase is divided among a fixed number of $\sum_{i=1}^{N} M_i$ (or with our simplifying assumption N×M) size groups, each representing a range of bubble sizes and where break-up and coalescence between all size groups is taken into account. Introducing r_G and ρ_G as the volume fraction and density of the cumulative disperse gaseous phase and $r_i=r_G \cdot f_i=r_\alpha \cdot f_{\alpha,i}$ the gas volume fraction in a single size group, then the continuity equations for the velocity group α, $\alpha \in [1,N]$ and the bubble size group i, $i \in [1,N\times M]$ read:

$$\frac{\partial}{\partial t}\left(\rho_G r_\alpha\right)+\frac{\partial}{\partial x^j}\left(\rho_G r_\alpha U_\alpha^j\right)=S_\alpha \tag{16}$$

$$\frac{\partial}{\partial t}\left(\rho_G r_\alpha f_{\alpha,i}\right)+\frac{\partial}{\partial x^j}\left(\rho_G r_\alpha f_{\alpha,i} U_\alpha^j\right)=S_{\alpha,i} \tag{17}$$

with the additional relations and constraints:

$$\begin{aligned} r_G &= \sum_{\alpha=1}^{N} r_\alpha = \sum_{i=1}^{N\times M} r_i \quad , \quad r_\alpha = \sum_{i=1}^{M_\alpha} r_i\Big|_{vel.group\,\alpha} \\ r_L + r_G &= 1 \quad , \quad \sum_{i=1}^{N\times M} f_i = 1 \quad , \quad \sum_{i=1}^{M_\alpha} f_{\alpha,i}\Big|_{vel.group\,\alpha} = 1 \end{aligned} \tag{18}$$

Here in eq. (17) the term $S_{\alpha,i}$ is the net rate at which mass accumulates in group i due to coalescence and break-up. This term can be written as:

$$\begin{aligned} S_{\alpha,i} &= B_{i,B} - D_{i,B} + B_{i,C} - D_{i,C} \\ &= \rho_G r_G \sum_{j>i} B_{ij} f_j - \rho_G r_G f_i \sum_{j<i} B_{ij} \\ &\quad + \left(\rho_G r_G\right)^2 \frac{1}{2} \sum_{j\le i} \sum_{k\le i} C_{jk} f_j f_k \frac{m_j + m_k}{m_j m_k} X_{jk\to i} - \left(\rho_G r_G\right)^2 \sum_j C_{ij} f_i f_j \frac{1}{m_j} \end{aligned} \tag{19}$$

with:

$$S_\alpha = \sum_{i=1}^{M_\alpha} S_{\alpha,i}\Big|_{vel.group\,\alpha} \quad , \quad \sum_{\alpha=1}^{N} S_\alpha = 0 \tag{20}$$

where $B_{i,B}$ is the bubble birth rate due to break-up of larger bubbles, $D_{i,B}$ is the bubble death rate due to break-up of bubbles from size group i into smaller bubbles, $B_{i,C}$ is the bubble birth rate into size group i due to coalescence of smaller bubbles to bubbles belonging to size group i and finally $D_{i,C}$ is the bubble death rate due to coalescence of bubbles from size group i with other bubbles to even larger ones. B_{ij} and C_{ij} are the break-up and coalescence rates of bubbles from size groups i with bubbles of size group j. In eq. (19) m_i denotes the mass of the disperse phase allocated to bubble size group i and $X_{jk\to i}$ is the fraction of mass transferred to size group i due to coalescence of two bubbles from size groups j and k. Applying the break-up model of Luo & Svendsen [7] and the coalescence model of Prince & Blanch [12], the terms of the bubble break-up and coalescence rates B_{ij} and C_{ij} can be defined in dependence on local gaseous phase velocity, size group and fluid turbulence properties.

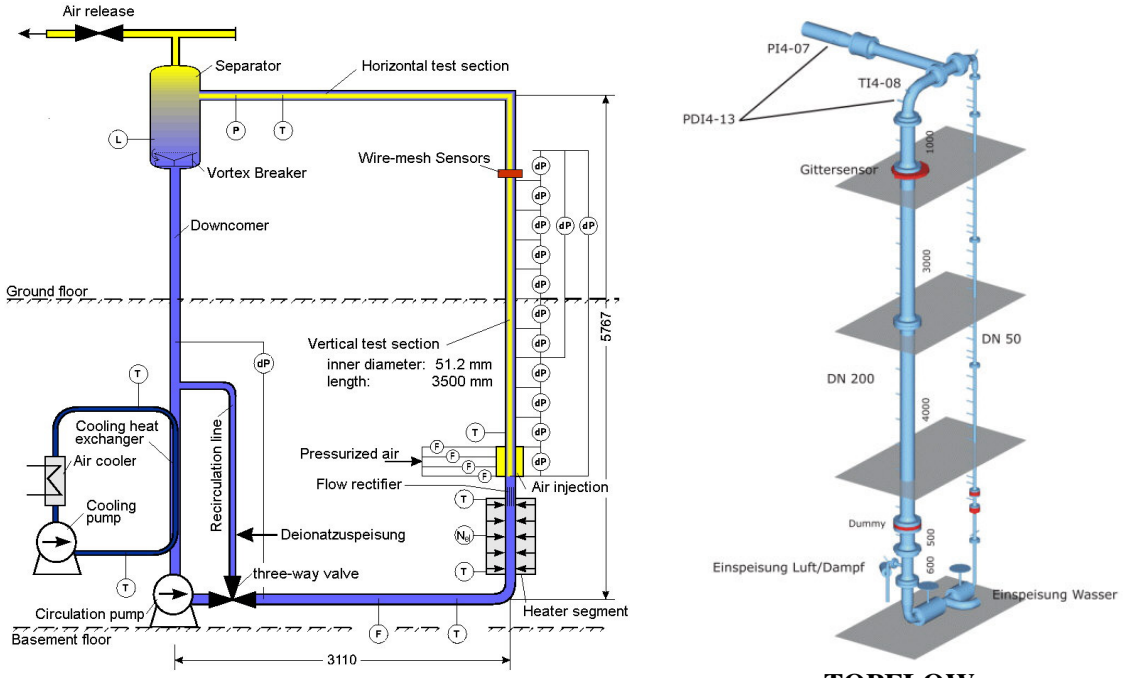

Fig. 2: MT-Loop and TOPFLOW test facilities at the Research Center Rossendorf (FZR), Germany for vertical pipe flow investigations on air-water and steam-water two-phase flows.

FZR Test No.	$\bar{d}_P[mm]$	$U_{L,\sup}[m/s]$	$U_{G,\sup}[m/s]$
017	4.8	0.405	0.0040
019	4.8	1.017	0.0040
030	4.4	1.017	0.0062
038	4.3	0.225	0.0096
039	4.5	0.405	0.0096
040	4.6	0.641	0.0096
041	4.5	1.017	0.0096
042	3.6	1.611	0.0096
074	4.5	1.017	0.0368

Table 1: Test conditions for experimental investigations at the MT-Loop test facility

Grid level	No. of grid elements in pipe cross section	No. of grid elements along pipe axis	No. of grid elements
1	192	82	15 744
2	320	100	32 000
3	500	128	64 000
4	819	158	129 402
5	1 280	200	256 000

Table 2: Hierarchy of numerical meshes

Model Validation for Monodisperse Gas-Liquid Bubbly Flows

The MT-Loop Test Facility and Database

Numerical simulation data has been validated [4] against extensive experimental results for air-water bubbly flows available from a FZR database [9], [10]. The measurements at the MT-Loop test facility (Fig. 2) were carried out at a vertical test section of 4m height and 51.2mm inner diameter. Air bubbles were injected into an upward water flow at normal conditions using a sparger with 19 capillaries equally distributed over the pipe cross section. A large number of tests with different ratios of air and water superficial velocities resulting in a slightly varying bubble diameter were performed (Tab. 1). In the tests used for the current validation the loop was operated with air at atmospheric pressure and 30°C temperature. Stationary conditions were settled for each experiment. Gas void fraction profiles were measured at a height of 3.08m above the air injection using a fast wiremesh sensor developed at FZR [9], [10] with 24x24 electrodes. Additionally bubble size and void fraction distributions are available for 10 different measurement cross sections at different L/D=0.6,...,59.2.

a)

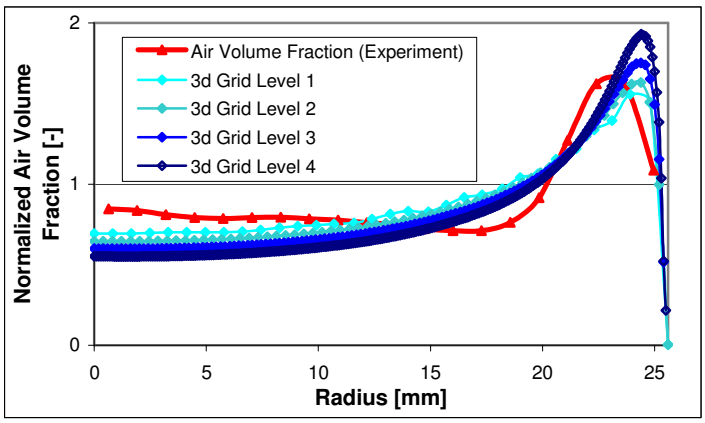

b)

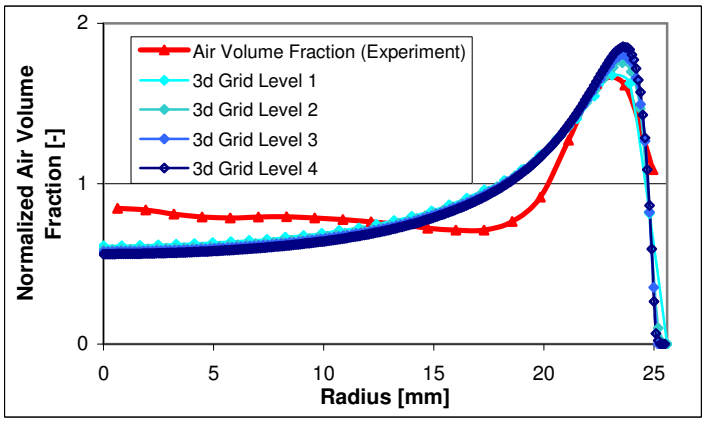

Fig. 3: Grid independence of numerical results for test case MT-Loop 074 using a) Antal's wall lubrication force and b) Tomiyama's wall lubrication force.

BPG Study of the Baseline Test Case MT-Loop 074

The numerical simulations had been carried out in accordance with the Best Practice Guidelines (BPG) for CFD code validation [8]. For the vertical pipe flow geometry shown in Fig. 2 radial symmetry has been assumed, so that the numerical simulations could be performed on a 60^o radial sector of the pipe with symmetry boundary conditions at both sides. Inlet conditions were assumed to be homogeneous in terms of superficial liquid and gas velocities and volume fractions for both phases in accordance with the experimental setup conditions from Tab. 1. For the disperse bubbly phase a mean bubble diameter was specified, which was determined from the test case wiremesh sensor data. Consequently a monodisperse two-phase model has been used for the CFD simulation of test cases. At the outlet cross section of the 3.8m long pipe section an averaged static pressure outlet boundary condition was used.

A hierarchy of 5 numerical grids was constructed, where the number of grid elements has been increased by a factor of 2 from a coarser to a finer mesh (scaling factor of $2^{1/3}$ in each coordinate direction, see Tab. 2). The numerical meshes used local refinement towards the outer pipe wall, while min/max cell size and cell aspect ratios were kept almost constant for all different numerical grids. Dimensionless y^+ values varied between y^+=29.2 on the coarsest mesh and y^+=12.5 on the finest mesh.

First the above described monodisperse bubbly flow model including Grace drag law and non-drag force models for bubble lift, wall lubrication and turbulent dispersion forces have been applied to the MT-Loop test 074, which is the baseline case for all the following investigations. The full error hierarchy (round-off, discretization, iteration, solution and model error) has been studied in accordance with the BPG's [3], [6]. For investigation of flow solver convergence the gas holdup and the global mass balances for both phases in the vertical pipe were defined as monitored target variables. Reliable converged solutions could be obtained on all grid levels for a satisfied convergence criterion based on the maximum residuals of $1.0 \cdot 10^{-5}$ and for a physical time scale of the fully implicit steady-state (pseudo time stepping) solution method of Δt=0.005s.

For the comparison of the numerically predicted and measured gas volume fraction profiles at the uppermost measurement cross section of MT-Loop at z=3.03m (L/D=59.2) all data have been normalized:

$$r_G^*(x) = \frac{r_G(x)}{\frac{8}{D^2}\int_0^{D/2} r_G(x)\, x\, dx} \tag{21}$$

where x is the coordinate in radial direction and *D* is the pipe diameter.

Test case MT-Loop 074 has been investigated on the established 3-dimensional grid hierarchy in order to investigate the grid independence of the numerical solution. In this study Grace drag law, Tomiyama lift force, FAD turbulent dispersion force and the Sato model for bubble induced turbulence has been used. Fig. 3 shows two series of results for radial gas void fraction profiles at L/D=59.2 using either Antal's or Tomiyama's formulation of the wall lubrication force in the two-phase flow model. In Fig. 3b) numerical simulations give almost grid independent results for grid resolutions finer then the 2nd grid level, when Tomiyama's wall lubrication force formulation has been used. For the case with Antal's wall lubrication (Fig. 3a), grid independent results could not be obtained even on the 4th grid level. On grids with finer grid resolution the imbalance between Antal's wall lubrication force and Tomiyama's lift force leads to increasing amplitude of the wall peak in the gas volume fraction distribution, while the radial location of the void fraction maximum remains unchanged. A radial shift of the void fraction peak towards the wall can be observed in Fig. 3a) in comparison with the obtained void fraction distributions from Fig. 3b). This indicates that the wall lubrication force derived from Antal's

formulation seems too weak in order to balance Tomiyama's lift force at the correct radial location, so that the disperse phase is too much accumulated within a small number of grid cells near the wall.

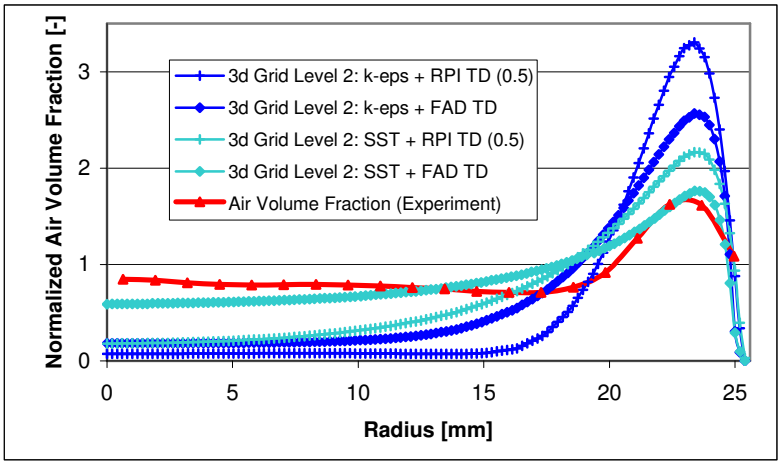

Fig. 4: Void fraction profiles for test case MT-Loop 074.

Further Fig. 4 shows the comparison of the predicted gas void fraction profiles on the 2nd grid level with experimental data of MT-Loop 074. In this comparison the turbulence model for the liquid phase has been varied from SST model with automatic wall treatment to Standard k-Epsilon model with wall functions [2]. Furthermore the turbulent dispersion force model for the gaseous phase has been varied between the FAD and the RPI model. It can be observed, that in all four simulations the balance between the Tomiyama lift and wall lubrication forces leads to a pronounced wall peak in the gas void fraction profile, which is the expected void fraction distribution for the given bubble diameter in this test case. On the other hand this wall peak is much too pronounced in comparison with the experimental data for the simulations using the standard k-ε turbulence model. Furthermore the turbulent dispersion of the disperse phase is underpredicted with the RPI model also resulting in too high gas void fraction values in the wall peak. Best results could be obtained with the combination of the SST turbulence model for the continuous phase using automatic wall function treatment [2] and the FAD TD model for the disperse phase in accordance with eq. (8). The higher turbulent dispersion of the FAD TD model leads not only to better agreement of void fraction data within the region of the wall peak but leads also to a substantial improvement of the void fraction distribution near the pipe axis.

Validation of Non-Drag Force Model Formulations for Varying Flow Conditions

A large number of validation tests have been carried out for varying flow conditions from the MT-Loop test case matrix [9], [10]. Fig. 5 shows the comparison of ANSYS CFX numerical simulations using the above described physical models for monodispersed bubbly flows with experimental data from the MT-Loop experiments at FZR. For the presented numerical simulations Grace drag law, Tomiyama lift force coefficient correlation and the FAD turbulent dispersion force model had been used, while the numerical results predicted with Antal, Tomiyama and Frank wall lubrication force models can be compared from the diagrams of Fig. 5.

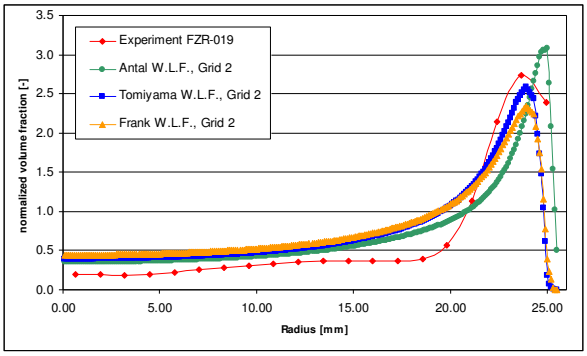

MT-Loop 019

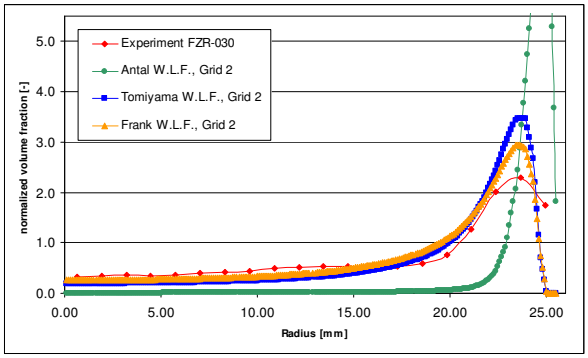

MT-Loop 030

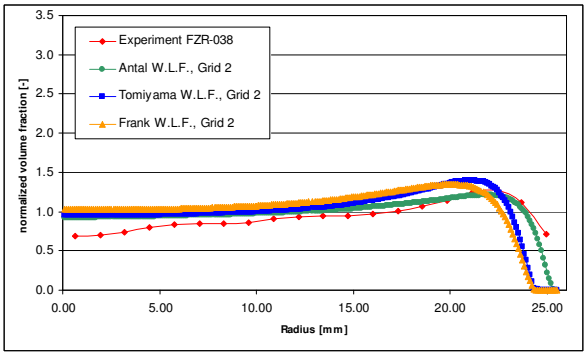

MT-Loop 038

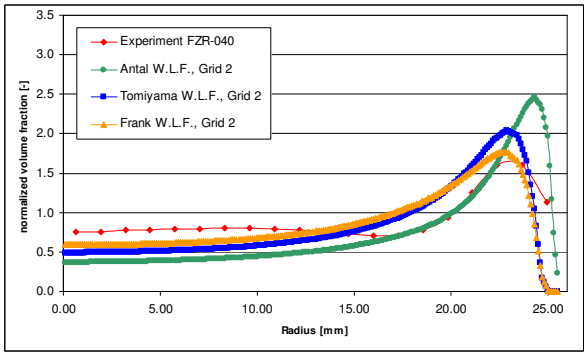

MT-Loop 040

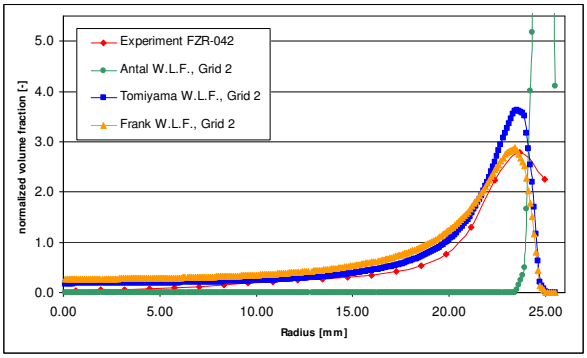

MT-Loop 042

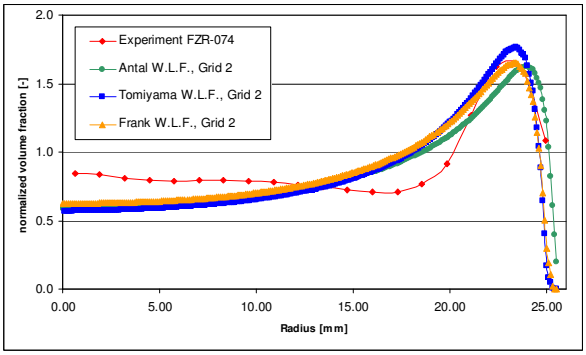

MT-Loop 074

Fig. 5: Comparison of CFX-5 numerical simulations vs. experimental results for varying MT-Loop flow conditions (see Tab. 1) using different wall lubrication force models.

For almost all investigated test cases the numerical results predicted with the generalized wall lubrication force formulation of eq. (15) are in very good agreement with the experimental data. These results using the Frank wall lubrication force model are close to the numerical solution given by the Tomiyama wall lubrication force as well, but simultaneously avoid the fixed geometrical length scale D of eq. (13). It can further observed that the Antal wall lubrication force formulation results in a gas volume fraction maximum of too high amplitude, which is located too close to the pipe wall for most test cases. Especially for test case conditions of FZR-030 and FZR-042 the Antal wall lubrication force is not able to balance the arising near

wall lift force acting on the bubbles, which leads to a strong overprediction in gas volume fraction maxima. Further results can be found in [4], [6], [9] and [10].

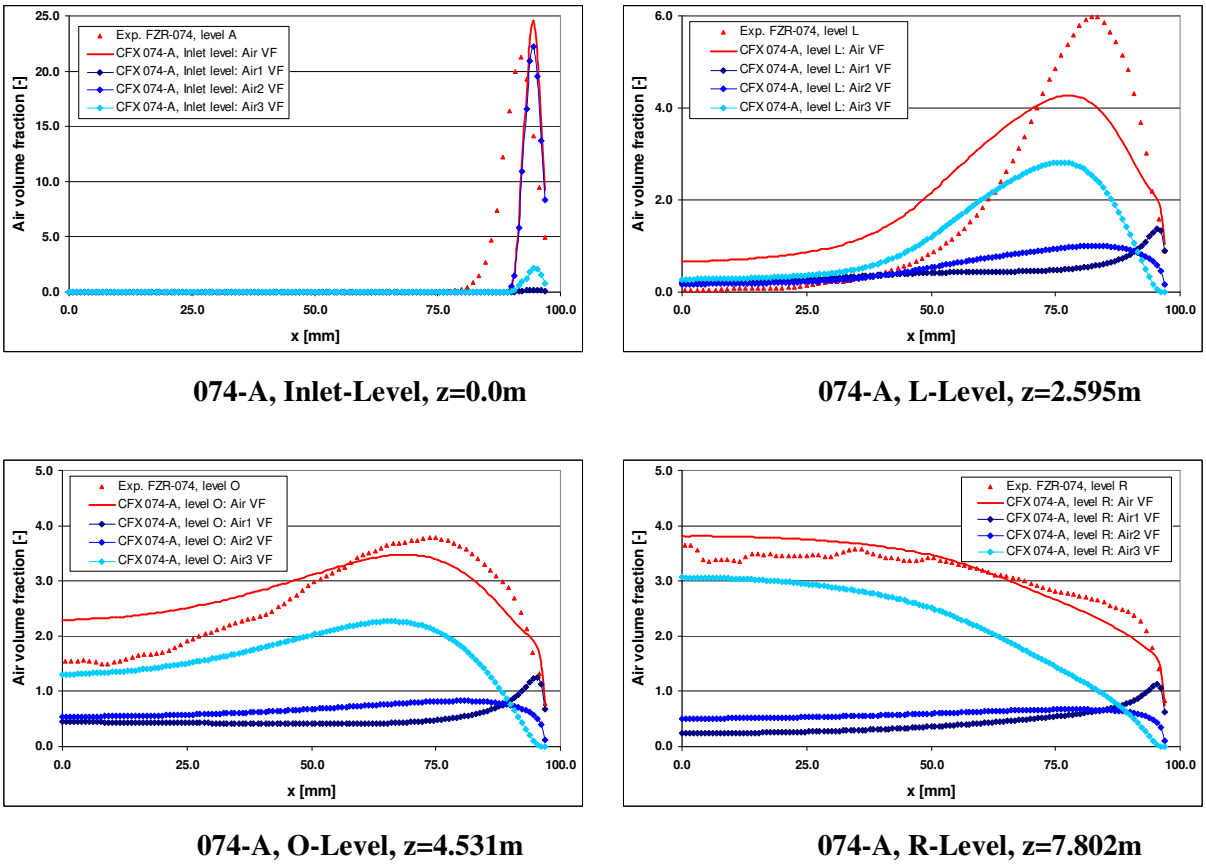

Fig. 6: Comparison of TOPFLOW-074 gas volume fraction measurements with CFX-10 inhomogeneous 3x7 MUSIG model prediction 074-A at different pipe elevation levels.

Model Validation for Polydisperse Gas-Liquid Bubbly Flows

The TOPFLOW Test Facility and Database

Experiments on the evolution of the radial gas fraction profiles, gas velocity profiles and bubble size distributions in a polydisperse gas-liquid two-phase flow along a large vertical pipe of D_I=194 mm inner diameter have been performed at the TOPFLOW facility [11] at FZ Rossendorf (Fig. 2). Two wire-mesh sensors were used to measure sequences of two-dimensional distributions of local instantaneous gas void fraction within the complete pipe cross-section with a lateral resolution of 3 mm and a sampling frequency of 2500 Hz. This data is the basis for fast flow visualization and for calculation of profile data, which have been used for comparison with the CFD simulations and further validation of the inhomogeneous MUSIG model. The gas void fraction profiles were obtained by averaging the sequences over time, velocities were measured by cross-correlation of the signals of the two sensors, which were located on a short (63 mm) distance behind each other. The high resolution of the mesh sensors allows identifying regions of

connected measuring points in the data array, which are filled with the gas phase. This method was used to obtain the bubble size distributions.

In the experiments, the superficial velocities ranged from J_G=0.04 to 8 m/s for the gas phase (air or vapor) and from J_L=0.04 to 1.6 m/s for the liquid, while the first model validation for the inhomogeneous MUSIG model was focused on the experiment TOPFLOW-074 with J_G=0.0368m/s and J_L=1.017m/s for an air-water flow. In this way, the experiments cover the range from bubbly to churn turbulent flow regimes, where the selected test case belongs to the range of bubbly flow with break-up and coalescence and a developed core peak in the gas volume fraction profiles for the largest distance between gas injection and measurement cross-section. The evolution of the flow structure was studied by varying the distance between the gas injection and the sensor position. This distance was changed by the help of a so-called variable gas injection set-up (see Fig. 2). It consists of 6 gas injection units, each of them equipped with three rings of orifices in the pipe wall for the gas injection. These rings are fed with the gas phase from ring chambers, which can be individually controlled by valves. The middle ring has orifices of 4 mm diameter, while the upper and the lower rings have nozzles of 1 mm diameter. In this way, 18 different inlet lengths and two different gas injection geometries can be chosen. The latter allows varying the initial bubble diameter at identical superficial velocities. For the test case 074 the 1mm orifices were used for gas injection. Therefore the development of the air-water flow can be studied from level R injection at z=7.802m below the wire-mesh sensor up to level A injection at z=0.221m below the measurement cross-section.

Flow Setup for Test Case TOPFOW-074

For a first validation study of the inhomogeneous MUSIG model the test case TOPFLOW-074 has been selected, which is characterized by superficial air and water velocities of J_G=0.0368m/s and J_L=1.017m/s, an isothermal temperature of 30°C and normal pressure. The pipe averaged gas volume fraction is still rather low for this test case at about r_G~3.5%. Nevertheless in large diameter pipes radial demixing of bubbles of different size or the present inlet BC's of gas injection can lead to locally high void fractions of more then 20% and break-up and coalescence processes gain in importance. For the vertical pipe flow geometry shown in Fig. 2, radial symmetry has been assumed, so that the numerical simulation was performed on a 60° radial sector of the pipe with symmetry boundary conditions (BC's) at both sides. At the outlet cross-section of the 10.0m long pipe section an averaged static pressure outlet BC has been applied. The pipe wall was assumed to be hydrodynamically smooth with a no-slip BC for water and a free-slip BC for the gaseous phase. The BC's for the SST turbulence model have been treated by the automatic wall function treatment of CFX-10 [2].

The inlet BC's for the liquid phase (water) at z=-2.0m correspond to water velocity, turbulent kinetic energy and turbulent eddy frequency profiles of a fully developed single-phase pipe flow. The air void fraction at the inlet cross-section of the pipe has been set to zero. Gas is injected at z=0.0m by point sources corresponding to the 12 individual 1mm wall orifices evenly distributed along the circumferential pipe wall of the 60° radial pipe sector. The injection velocity was calculated from the cross-section of the 1mm orifices and the gas mass flow defined by the given air superficial velocity.

For this first validation study of the inhomogeneous MUSIG model it was assumed, that the gaseous phase can be represented by 3 inhomogeneous velocity groups/phases with 7 bubble size classes in each group. Therefore an overall number of 21 bubble size classes have been used for the representation of the local bubble size distribution. The choice of 3 velocity groups was stimulated by the dependency of the Tomiyama lift force coefficient on the bubble diameter. This functional dependency shows for small bubbles a constant positive value of C_L, for large bubbles

a constant negative value of C_L and an intermediate range of linear change of the lift force coefficient with increasing bubble diameter. Otherwise previous investigations had shown, that at least 15 bubble size groups are necessary for a certain accuracy of the break-up and coalescence models in the MUSIG model. The choice of 7 bubble size groups per velocity group is therefore a compromise between accuracy in the representation of the bubble size distribution and the resulting numerical effort for the solution of the large system of differential equations.

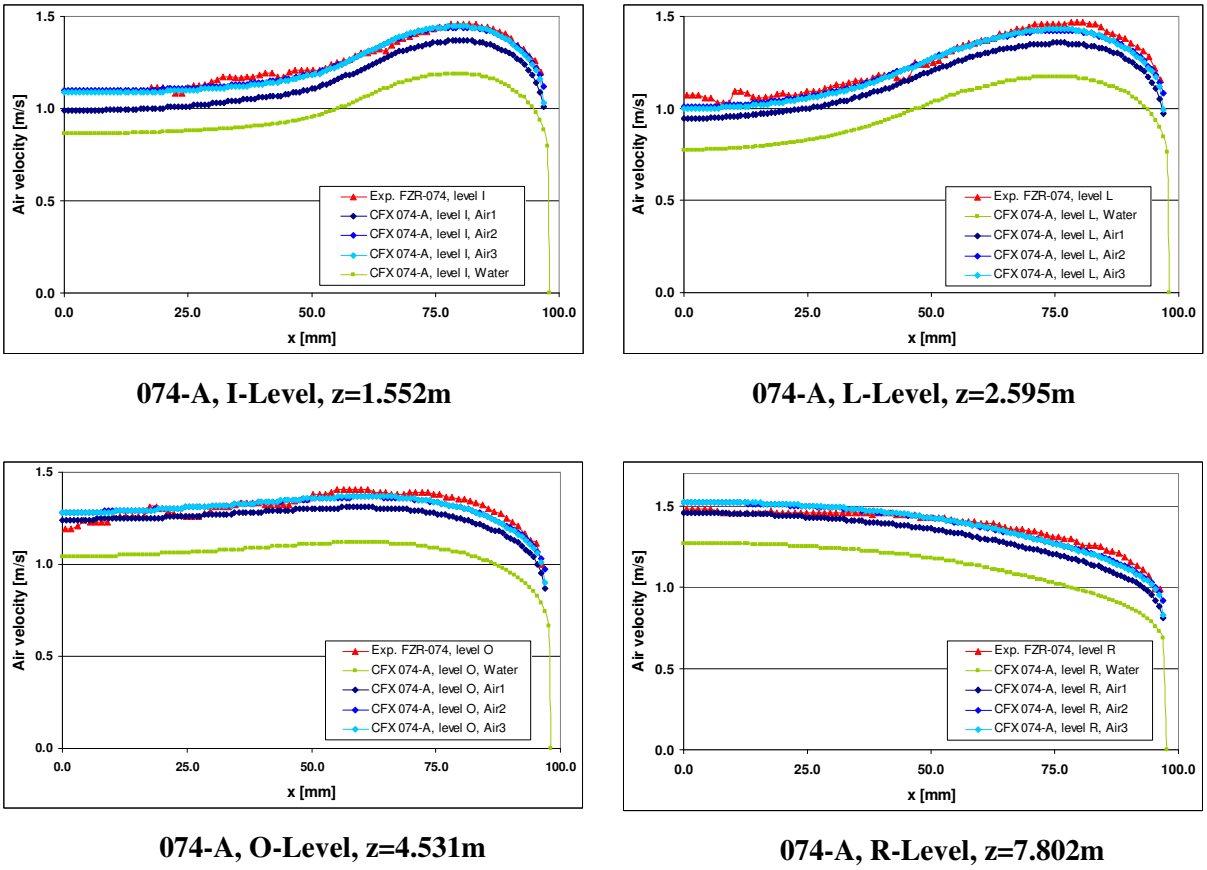

074-A, I-Level, z=1.552m

074-A, L-Level, z=2.595m

074-A, O-Level, z=4.531m

074-A, R-Level, z=7.802m

Fig. 7: Measured and predicted (simulation 074-A) radial water and air velocity profiles for the TOPFLOW FZR-074 test case at the I-, L-, O- and R-level.

The 21 bubble size classes were distributed according to an equal bubble diameter distribution with Δd_P=0.619mm over the bubble size range of d_P=0.01mm,…,13mm. The volume or size fraction distribution over these 21 bubble size classes for the wall orifice boundary conditions at z=0.0m was derived from the level A gas volume fraction and bubble size measurements of TOPFLOW-074, i.e. for the smallest available distance between gas injection and measurement location in the experiments. The mean bubble diameter at gas injection location is about d_P~6.5mm and the narrow bubble size distribution is similar to a Gaussian profile.

A full BPG study of the test case TOPFLOW-074 for the inhomogeneous MUSIG model was not carried out due to the large computational effort, which is necessary for the numerical simulation in this case. Nevertheless the results from the BPG investigations of the MT-Loop test

cases for monodisperse bubbly flows had been used as a starting point for the present investigation with respect to grid resolution, model setup and iteration/convergence parameters. The steady-state flow simulation was therefore carried out on a hexahedral mesh generated with ICEM/CFD consisting of approx. 260.000 elements and 278.000 nodes. Geometric grid refinement had been applied to the near wall region and to the area of developing gas-liquid flow above the point of gas injection. The steady state simulation with a physical timescale of dt=0.001s had run for 5500 iterations on 8 AMD Opteron processors with a memory consumption of about 4.8 Gbyte and a simulation time of approx. 11 days.

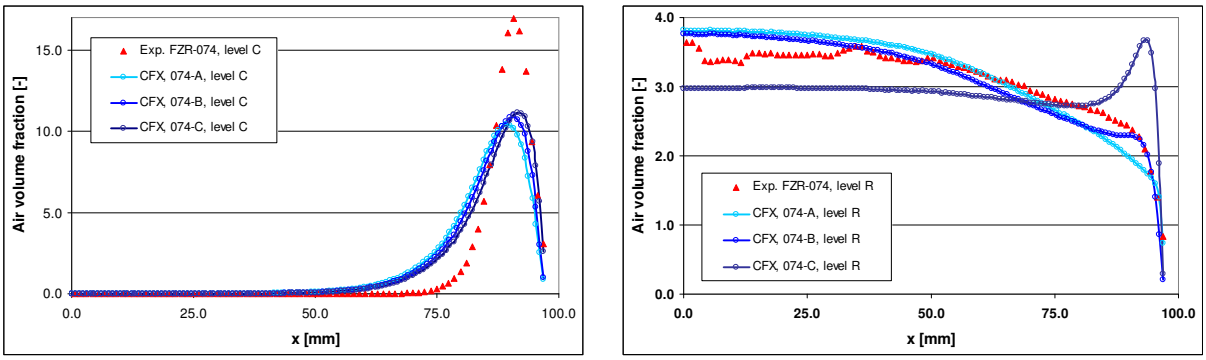

C-Level, z=0.335m **R-Level, z=7.802m**

Fig. 8: Comparison of cumulative radial air volume fraction profiles for TOPFLOW-074 test case simulations 074-A, -B and -C at the C- and R-level.

CFD Simulation and Comparison to Data for Test Case TOPFLOW-074

Three different simulations have been carried out for the presented test case TOPFLOW-074 and have been compared with experimental data:

- ***074-A***: bubble drag is calculated in correspondence with the Sauter mean diameter of a velocity group using Grace drag law [2]; a high void fraction correction exponent of 4.0 was used, while the correction was based on the local void fraction of the velocity group; break-up model of Luo & Svendson [7] and coalescence model of Prince & Blanch [12] were used without changes to the break-up and coalescence rates.
- ***074-B***: bubble drag is calculated according to the Tomiyama drag correlation [14] using a high void fraction correction exponent of 4.0, while the correction is based on the local but cumulative air void fraction of the disperse phase; unchanged settings for the break-up and coalescence model parameters in comparison with 074-A.
- ***074-C***: Since too high coalescence rates could be observed in simulations 074-A and 074-B, we reduced for this simulation the coalescence rates given by the Prince & Blanch model by a factor of 0.25 in order to study the model parameter influence on radial gas volume fraction distributions.

Results of the 074-A, 074-B and 074-C test case simulations are compared to gas volume fraction and gas velocity measurements at different elevations of the TOPFLOW test facility. In Fig. 6 and Fig. 9 each volume fraction profile of a velocity group (disperse phase) has been calculated as the cumulative sum of the volume fraction profiles of 7 corresponding bubble size classes. The cumulative air volume fraction profiles as compared in Fig. 8 represent the sum of gaseous phase void fraction over all 21 bubble size classes. Fig. 6 shows the axial development

of the gas-liquid bubbly flow from the gas injection through wall orifices up to the uppermost measurement cross-section at R-level (simulation 074-A). At the injection level the gaseous phase is almost concentrated in a near wall bubble plume, where local gaseous phase volume fraction reaches as high levels as about 25%. Due to the prescribed inlet BC's gaseous phase belongs nearly entirely to the 2nd velocity group, while only a minor part of gas void fraction can be observed in the 3rd velocity group of large bubbles.

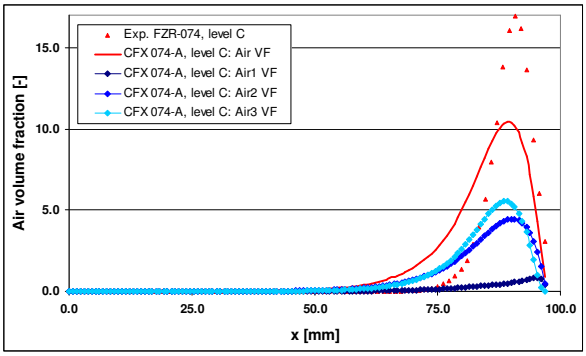

074-A, C-Level, z=0.335m

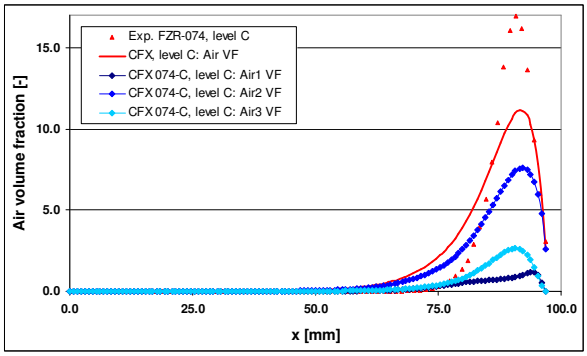

074-C, C-Level, z=0.335m

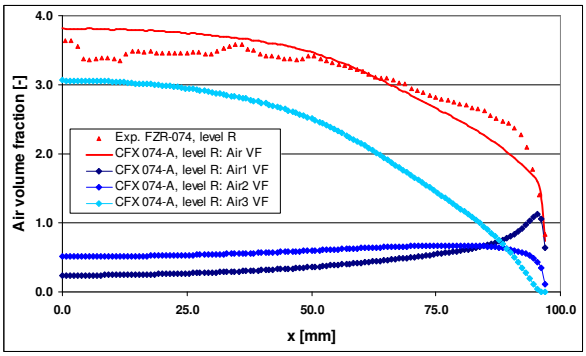

074-A, R-Level, z=7.802m

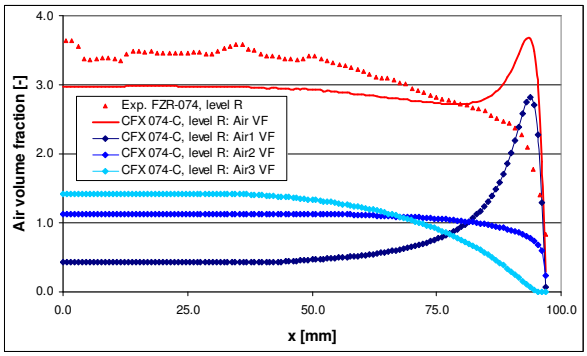

074-C, R-Level, z=7.802m

Fig. 9: Comparison of homogeneous volume group resolved radial volume fraction profiles for TOPFLOW-074 test case simulation 074-A and 074-C at C- and R- levels.

Further diagrams in Fig. 6 show the axial development of the bubble plume arising from the wall orifices. At the same time, while the gas bubble plume is spreaded radially inwards by turbulent dispersion, coalescence of bubbles takes place leading to an increasing gas volume fraction in the bubble size classes with larger bubble diameters (in the velocity group Air3). Simultaneously large bubbles are decaying into smaller ones due to bubble break-up in boundary layer turbulence close to the wall. At the uppermost measurement cross-section at the R-level small bubbles (Air1) show a slightly pronounced wall peak, medium sized bubbles (Air2) are almost homogeneously distributed over the pipe cross section, while for the large bubbles (Air3) a remarkable core peak in the gas volume fraction profiles can be observed. The cumulative gas volume fraction profile finally shows a core peak, since most of the gaseous phase volume fraction had been reallocated to the velocity group of large bubbles due to coalescence. Also it

can be observed that the gas bubble plume injected through the wall orifices is spreading a little bit too fast, the established accuracy and agreement with the experimental data for the axial development of gas volume fraction profiles is remarkably good with respect to the complexity of the flow.

Fig. 7 shows the comparison of radial velocity profiles of the liquid phase and velocity groups with measured gas velocities (074-A). The agreement is very good at all pipe elevation levels. Especially for the lower I- and L-levels a near wall deformation of the radial water velocity profile due to the wall orifice gas injection and the buoyancy of the developing gas bubble plume can be observed. In fully developed state at R-level the water velocity profile is then again comparable to fully developed turbulent pipe flow profile. The smaller slip velocity of the small bubbles velocity group is caused by the higher drag of small bubbles.

If we look on the distribution of the cumulative gas volume fraction over the three velocity groups, then it could be observed from 074-A simulation results (Fig. 6), that a too high void fraction was finally found in the large bubbles velocity group (Air3) due to a too strong coalescence. Furthermore it was observed, that the initial near wall bubble plume was spreaded too fast in terms of radial propagation and lowering of the maximum void fraction. This both observations gave rise to further investigations of 074-B and 074-C simulations.

Fig. 8 shows the direct comparison of the cumulative gaseous phase volume fraction profiles for these three simulation runs. It can be observed from the C-level diagram, that the changes in high void fraction bubble drag coefficient correction and related turbulent dispersion force changes had almost no effect on the cumulative void fraction distribution at lower pipe elevations. Otherwise the reduced coalescence rates in 074-C lead to a higher amount of gas volume fraction in the small bubble velocity group (Air1) due to relatively more pronounced break-up processes. Since small bubbles are shifted by lift force towards the pipe wall we can observe a near wall maximum in the gas volume fraction profile at the R-level.

Fig. 9 highlights the effect of reduced coalescence rates in 074-C in more detail by comparing the velocity group resolved volume fraction profiles with 074-A simulation results. While in 074-A the void fraction accumulated in Air2 and Air3 is almost equal at C-level, the same gas volume fraction profile is still dominated by the Air2 volume fraction distribution for 074-C simulation. High coalescence rates in 074-A lead to a shift of about 75% of overall gas volume fraction to the large bubble velocity group (Air3). In contrary for 074-C gas volume fraction is almost evenly distributed amongst the three velocity groups, but unfortunately leading to a non-physical near wall void fraction maximum and lowered void fraction level in the pipe core. Best agreement with experimental data was therefore established for the 074-B simulation conditions and more detailed investigations of the turbulent dispersion, break-up and coalescence models are necessary in order to resolve the remaining differences.

Conclusion

The paper presents model derivation and validation for mono- and polydisperse gas-liquid bubbly flows taking into account drag and non-drag interfacial momentum transfer. For polydisperse bubbly flows the so-called inhomogeneous MUSIG model is introduced, which allows to split the gaseous phase into N velocity groups. Therefore this model is capable to predict for the radial demixing of bubbles of different sizes due to acting lift forces of different radial direction. The development of the polydisperse bubble size distribution is predicted by splitting each of the N velocity groups into M bubble size classes and by accounting for bubble break-up and coalescence processes.

Developed Eulerian multiphase flow models have been applied to two series of test cases based on MT-Loop and TOPFLOW experiment databases from FZ Rossendorf. The numerical

simulations have been carried out in accordance with Best Practice Guidelines [8] as far as applicable. Different sources of errors (round-off, discretization, iteration, solution and model error) have been investigated for the baseline test case MT-Loop-074. Applying the established reliable convergence parameters to varying flow conditions of other MT-Loop test cases, the model error of liquid phase turbulence models, turbulent dispersion force models and wall lubrication force models have been quantified. Very good agreement of CFD predictions with experimental data have been found for most test case conditions using Tomiyama lift force, the generalized wall lubrication force formulation by Frank, FAD turbulent dispersion force and SST turbulence modeling for the liquid phase together with Sato's bubble induced turbulence model.

Furthermore in a first validation of the inhomogeneous MUSIG model the TOPFLOW-074 test case has been investigated using the knowledge gained from the BPG study of the baseline test case MT-Loop-074. Good agreement with experimental data has been obtained using a 3×7 inhomogeneous MUSIG model. The axial development of the gas-liquid bubbly flow from initial gas void fraction profile showing a pronounced near wall peak to flow conditions with a core peak in the gas void fraction profile has been successfully predicted. Nevertheless remaining differences between CFD results and experimental data need further investigation and improvements to the bubble break-up and coalescence models.

For the intended application of the derived multiphase flow models to the flow prediction in LWR fuel rod bundles further investigations, model development and validation are necessary. The inhomogeneous MUSIG model has to be further extended in order to account for changes in the bubble size distribution due to condensation and evaporation processes. Furthermore the polydisperse bubbly flow models have to be combined with an appropriate wall boiling model.

Acknowledgements

This research has been supported under contract number 150 1271 by the German Ministry of Economy and Labour (BMWA) in the framework of the German CFD Network on Nuclear Reactor Safety Research and Alliance for Competence in Nuclear Technology, Germany.

References

[1] Antal S.P., Lahey R.T., Flaherty J.E.: "Analysis of phase distribution in fully developed laminar bubbly two-phase flow", *Int. J. Multiphase Flow*, Vol. 7, pp. 635-652, 1991.

[2] CFX-10 User Manual, ANSYS-CFX, July 2005.

[3] Frank Th.: "Bubble flow in vertical pipes – Investigation of the testcase VDL-01/1 (FZR-074) for the validation of CFD", ANSYS CFX Germany, Technical Report No. TR-03-09, pp. 34, October 2003.

[4] Frank Th., Shi J., Burns A.D.: "Validation of Eulerian multiphase flow models for nuclear reactor safety applications", 3rd International Symposium on Two-phase Flow Modelling and Instrumentation, Pisa, 22.-24. Sept. 2004.

[5] Frank Th.: "Advances in Computational Fluid Dynamics (CFD) of 3-dimensional gas-liquid multiphase flows", NAFEMS Seminar "Simulation of Complex Flows (CFD), Wiesbaden, Germany, April 25-26, 2005, pp. 1-18.

[6] Frank Th.: Abschlußbericht zum Forschungsvorhaben 150 1271 „Entwicklung von CFD-Software zur Simulation mehrdimensionaler Strömungen im Reaktorkühlsystem", Technical Report TR-06-01, ANSYS Germany, Otterfing, January 2006, pp. 72.

[7] Luo H., Svendsen H.F.: "Theoretical model for drop and bubble break-up in turbulent dispersion", *AIChE J.,* Vol. 42, No. 5, pp. 1225-1233, 1996.

[8] Menter F.R.: "CFD Best Practice Guidelines (BPG) for CFD code validation for reactor safety applications", EC Project ECORA, Report EVOL-ECORA-D01, pp. 1-47, 2002.

[9] Prasser H.M., Lucas D., Krepper E., Baldauf D., Böttger A., Rohde U. et al.: „Strömungskarten und Modelle für transiente Zweiphasenströmungen", Forschungszentrum Rossendorf, Germany, Report No. FZR-379, pp. 183, June 2003.

[10] Lucas D., Krepper E., Prasser H.-M.: "Development of co-current air-water flow in vertical pipe", Int. J. Multiphase Flow, Vol. 31, pp. 1304-1328, 2005.

[11] Prasser H.-M., Beyer M., Carl H., Gregor S., Lucas D., Schütz P., Weiss F.-P.: "Evolution of the Structure of a Gas-Liquid Two-Phase Flow in a Large Vertical Pipe", The 11th International Topical Meeting on Nuclear Reactor Thermal-Hydraulics (NURETH-11), Popes Palace Conference Center, Avignon, France, October 2-6, 2005.

[12] Prince M.J., Blanch H.W.: "Bubble coalescence and break-up in air-sparged bubble columns", *AIChE J.,* Vol. 36, No. 10, pp. 1485-1499, 1990.

[13] Tomiyama A.: "Struggle with computational bubble dynamics", ICMF'98, 3rd Int. Conf. Multiphase Flow, Lyon, France, pp. 1-18, June 8.-12. 1998.

[14] Tomiyama A.: "Single bubbles in stagnant liquids and in linear shear flows", Workshop on Measurement Technology (MTWS5), FZ Rossendorf, Dresden, Germany, 2002, pp. 3-19.